Vol. 57, Issue 4, 371–386, 2024

Economic and Environmental Geology

THE KOREAN SOCIETY OF ECONOMIC AND ENVIRONMENTAL GEOLOGY

pISSN : 1225-7281
eISSN : 2288-7962

Research Paper

The Role of Organic Matter in Gold Occurrence: Insights from Western Mecsek Uranium Ore Deposit

Medet Junussov[1,*], Ferenc Mádai[2], János Földessy[2], Mária Hámor-Vidó[3]

[1]*Department of Geological Science, Faculty of Mining and Geosciences, Nazarbayev University, Astana 010000, Kazakhstan*
[2]*Institute of Mineralogy and Geology, Faculty of Earth Sciences and Engineering, University of Miskolc, H-3515 Miskolc-Egyetemváros, Hungary*
[3]*Department of Geology and Meteorology, Institute of Geography and Earth Sciences, Faculty of Sciences, University of Pécs, H-7622 Pécs, Vasvári pál utca, Hungary*

*Corresponding author : medet.junussov@nu.edu.kz

ARTICLE INFORMATION

Manuscript received 5 April 2024
Received in revised form 2 August 2024
Manuscript accepted 22 August 2024
Available online 30 August 2024

DOI : http://dx.doi.org/10.9719/EEG.2024.57.4.371

Research Highlights

- Gold content has occurred in organic matter as metal-organic compounds of carbonaceous sedimentary rocks in the Western Mecsek uranium ore deposit
- The organic matter has a crucial role in the concentration, transportation, and preservation of the gold, uranium, and sulfur in the deposit.
- Enrichments of gold have been confirmed in the organic matter-rich reducing zones in pyrobitumen and arsenian pyrite

ABSTRACT

This paper presents analytical insights regarding into the occurrence of gold within organic matter, which is hosted by solid bitumen and closely associated with uranium ores in the Late Permian Kővágószőllős Sandstone Formation in Western Mecsek, South-West Hungary. The study utilizes a range of analytical techniques, including X-ray powder diffraction (XRPD) and wavelength dispersive X-ray fluorescence (WD-XRF) for comprehensive mineralogical and elemental analysis; organic petrography and electron microprobe analysis for characterizing organic matter; and an organic elemental analyzer for identifying organic compounds. A three-step sequential extraction method was used to liberate gold from organic matter and sulfide minerals, employing KOH, HCl, and aqua regia, followed by inductively coupled plasma optical emission spectroscopy (ICP-OES) to quantify gold contents.

The organic matter is identified as comprising two vitrinite types (telinite V1 and reworked V2) and three solid bitumen forms: non-fluorescing (B1) and fluorescing (B2) fillings within the V1, as well as homogenous pyrobitumen (PB) occupying narrow cracks and voids within globular quartz. Despite the samples exhibiting low total organic carbon content (<1 wt%), they display high sulfur content (up to 6 wt%) and the sequentially extracted noble metal content from the organic matter is found to total 7.45 ppm gold.

The research findings suggest that organic matter plays crucial roles in ore mineralization processes. Organic matter acts as an active component in the migration of gold, uranium, and hydrocarbons within sulfur-rich hydrothermal fluids. Additionally, organic matter contributes to the entrapment and enrichment of gold in hetero-atomic organic fractions, forming metal-organic compounds. Moreover, uranium inclusions are observed as oxide/phosphate minerals within solid bitumen and associated vitrinite particles. These insights into the occurrence and distribution of gold within organic matter highlight substantial exploration potential, guiding additional research activities focused on organic matter within the Kővágószőllős Sandstone Formation at the Western Mecsek deposit.

Keywords: pyrobitumen, vitrinite, gold, metal-organic compounds, Western Mecsek

Citation: Junussov, M., Mádai, F., Földessy, J., Hámor-Vidó, M. (2024) The Role of Organic Matter in Gold Occurrence: Insights from Western Mecsek Uranium Ore Deposit. Korea Economic and Environmental Geology, v.57, p.371-386, doi:10.9719/EEG.2024.57.4.371.

Journal homepage: http://www.kseeg.org/main.html

Econ. Environ. Geol., 57(4), 371-386, 2024
http://dx.doi.org/10.9719/EEG.2024.57.4.371

pISSN 1225-7281
eISSN 2288-7962

1. Introduction

Two terms are frequently used in the literature to describe the association of gold with organic matter in ore deposits. Some publications refer to “metal-organic compounds” or complexes, where metal cations are bonded to non-carbon atoms, typically oxygen, sulfur, or nitrogen, within organic ligands (Giordano and Kharaka 1994; Junussov et al. 2021, 2024). Conversely, other authors use the term "metalliferous coal" to denote gold-containing occurrences across various coal ranks from lignite to sub-bituminous coal (Hower et al. 2000). In this study, the term “metal-organic compounds” are preferred.

The investigation of gold as a metal-organic compound has been conducted by several authors (Emsbo and Koenig 2007; Ross et al. 2011; Migdisov et al. 2017; Junussov et al. 2021) across coal, bitumen, and thermally altered solid bitumen (or solid pyrobitumen) in ore deposits. According to Jacob (1989) and Glikson et al. (2000), pyrobitumen is identified as a high-temperature product derived from solid bitumen, characterized by its high aromaticity and insolubility, with a vitrinite reflectance (Ro%) exceeding 2%. Pyrobitumen typically lacks fluorescence or exhibits weak brown fluorescence at wavelengths above 650 nm, and is often associated with magmatic activity and hydrothermal fluid convection (Simoneit 1994, 2000, 2018).

Moreover, the significance of organic matter in the migration and entrapment of gold has been highlighted by several authors (Simoneit 2000, 2018; Migdisov et al. 2017; Junussov et al. 2021). Phenolic aromatic and thiophenic sulfur compounds within hot aqueous ore fluids have been identified as key factors favoring metal occurrence (Giordano and Kharaka 1994; Giordano 2000; Junussov et al. 2021, 2024), particularly in sedimentary basins with diverse basement compositions including granites and volcanic rocks (Seredin and Finkelman 2008). The organic matter contains gold concentrations tens, hundreds, or even thousands of times greater than the Clark value (Seredin, 2007). Therefore, the anomalously high concentrations of gold in the organic-rich sedimentary basins may have economic potential for primary extraction or by-product recovery (Seredin, 2007; Seredin and Finkelman, 2008; Junussov, 2018).

Gold, along with a range of other metals, has been discovered in Hungarian coal deposits associated with uranium ores, as extensively documented (Varga et al. 1972; Kádas 1983). Hungarian coals, as described by Kádas (1983), have been found to contain gold concentrations of up to 2 ppm, accompanied by rare earth elements, with the highest being Y at 1000 ppm, predominantly within reduced varieties of Permian-Early Triassic sandstone formations. In these formations, metals associated with organic matter are bound through complexation and sorption processes facilitated by functional groups (Idiz et al. 1986). The favorable adsorption of metal humic acid promotes cation exchange within insoluble humic acid, leading to gold enrichment in areas with high uranium content, as described by Szalay (1969) and Barabás (1956; 2013).

The study aims to understand the role of organic matter in enriching gold within the deposit and to evaluate its economic potential for future exploration, through three objectives: (1) characterizing organic matter distribution, (2) studying its impact on gold migration and precipitation, and (3) developing a genetic model to explain the occurrence of gold associated with organic matter.

2. Geological Settings

2.1. The Regional and Deposit Geology

The Mecsek Mountains, located in the Southern Central region of Hungary, approximately 220 km south of Budapest, are a significant geological area with notable mineral deposits. The primary urban center in this region is Pécs city. Situated in the western part of the Mecsek Mountains is the Western Mecsek uranium ore deposit, covering approximately 177 square kilometers and prominently found near the village of Kővágószőlős. This uranium ore deposit is within the Late Permian Kővágószőllős Sandstone Formation (KSF), which is part of the Late Permian sediments within the Permian-Triassic anticline of the Mecsek Mountains (René, 2017).

Geologically, the Mecsek Mountains are situated in the southwestern part of the Tisza Mega-unit, forming the basement of the Eastern Pannonian Basin. This area belongs to the Variscan orogenic belt, which was accreted during the Carboniferous–Permian period (C-P) (Szederkényi et

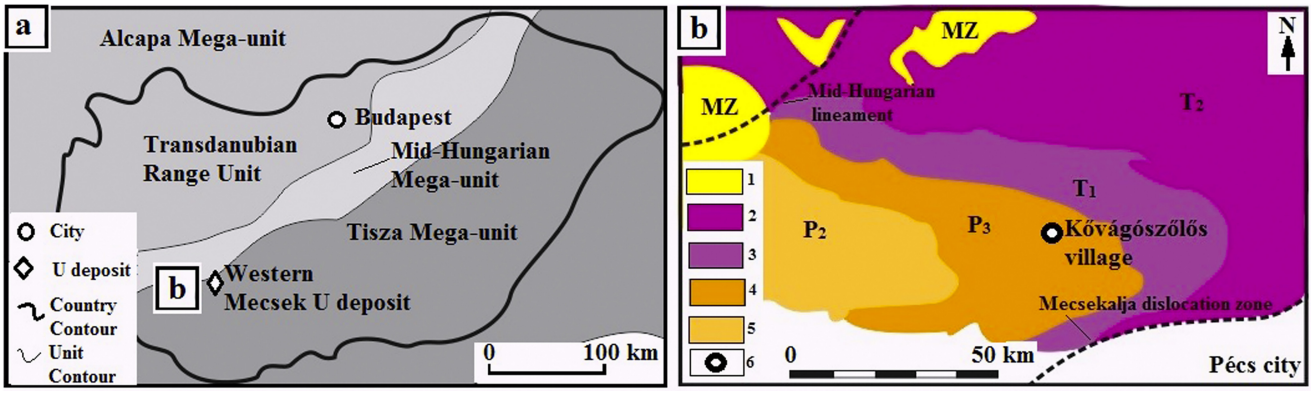

Fig. 1. Regional map (a) with main structural units (after Haas et al. 2010) and geological map (b) of the Western Mecesk uranium (U) deposit surrounding area of the Mecsek Mountains (after Barabás 2013), Legend: 1-Mezozoic; 2-Middle Triassic sandstone and siltstone; 3- Early Triassic conglomerate and sandstone; 4-Late Permian Kővágószőllős Sandstone Formation (KSF) including 4 members (Cserkút, Tótvár, Kővágótöttös and Bakonya); 5-Middle Permian claystone and conglomerate (Boda and Cserd); 6-Kővágószőlős village.

al., 2012). The Tisza Mega-unit comprises the basement of the Eastern Pannonian Basin, including parts of Transdanubia and Mid-Hungarian, as well as the northern portion of the Mecsekalja strike-slip fault zone (Szederkényi et al., 2012), shown in Fig. 1a-b.

The Kővágószőllős Sandstone Formation (KSF) is of particular interest due to its uranium mineralization, which are of polygenic origin. The uranium ores within the KSF exhibit stratiform pennaccordance, disseminated, and transversal enrichments (Barabás, 2013). The sandstones within the formation display various colors such as grey, green, and red, reflecting different stages of a prolonged autochthonous mineralization process resulting from fluid infiltration (Vincze, 1987).

Uranium concentrations are typically found in the grey rocks or green lenses of sandstones between the grey and red zones (Barabás and Konrád, 2000). The thickness of uranium-bearing sandstone varies from 15 to 90 meters, with most ore bodies located at depths between 650 to 800 meters (Fodor, 1998). Presently, known uranium mineral resources in the area amount to 26.3 million metric tons, containing about 31,000 metric tons of metallic uranium, with an average uranium concentration of 0.117% (Fodor, 1998).

Limited analyses suggest the presence of gold in the sequence, particularly in intervals rich in reductive organic matter, with gold enrichment reaching a maximum of 6.5 grams per ton (g/t) (Földessy, 1998).

2.2. Stratigraphy

The stratigraphic sequence of the Western Mecsek, as described by many authors (Fazekas et al., 1987; Barabás 2013) includes the following formations (Fig. 2; described from the oldest to the youngest in order): Korpád Sandstone formation has about 300–320 meters thick, is predominantly red with variegated colors (red, grey, and green). It lies above the Mórágy Complex, a granite formation dated to 340–354 million years ago, characterized by high-K and Mg-rich plutonic rocks. The upper boundary of the Korpád Sandstone is eroded and covered by the Early Permian Gyűrűfű Rhyolite Formation, dating to around 266.8 million years ago. Gyűrűfű Rhyolite Formation comprises a volcanic body, 50–130 meters thick, displaying reddish-brown or reddish-purple hues. It directly overlays the eroded surface of the Korpád Sandstone. Cserdi Conglomerate formation with a thickness of 250–1000 meters, consists of fluvial conglomerates, sandstones, and siltstones. It overlies the eroded surface of the Gyűrűfű Rhyolite and gradually transitions into the Boda Siltstone Formation. Boda Siltstone Formation is discontinuously deposited throughout the basin. It transitions from the underlying Cserdi Conglomerate with transitional intervals, particularly in the northeastern direction and at the top of the formation. Kővágószőllős Sandstone Formation (KSF): This is the youngest lithostratigraphic unit, mainly containing uranium ores in its upper part. It ranges in thickness from 150 to 1400 meters and consists of four members: Bakonya

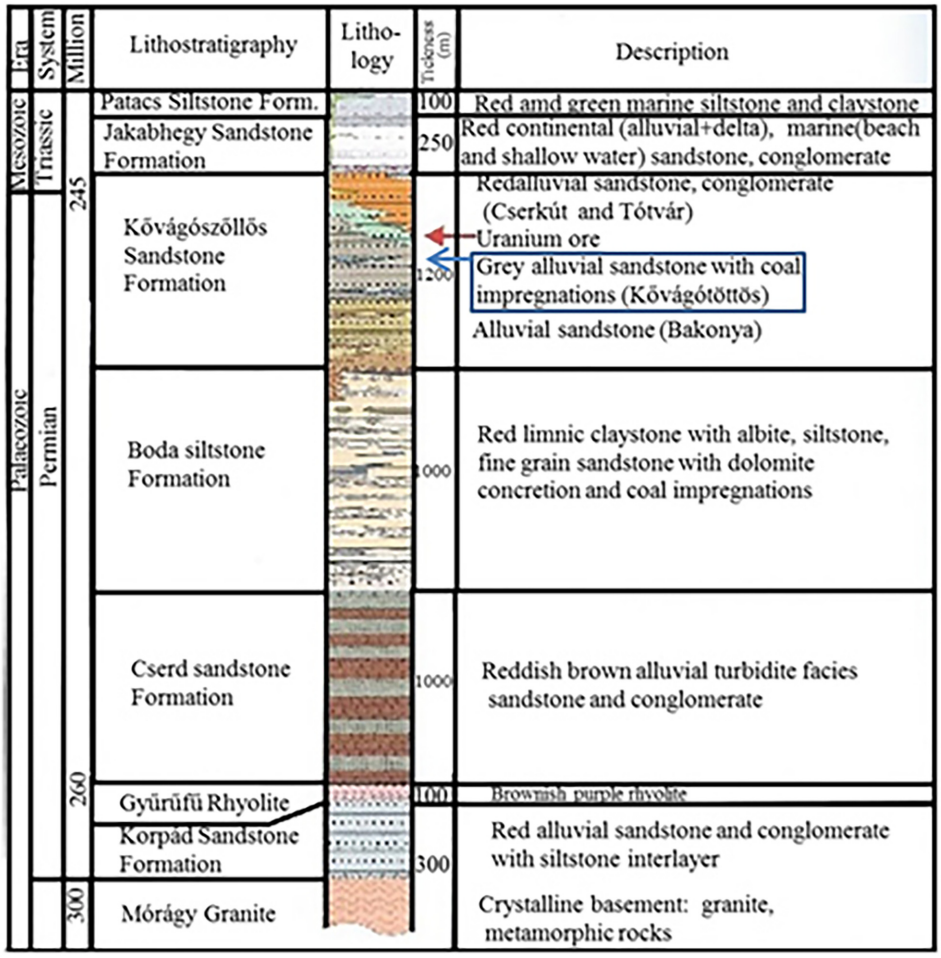

Fig. 2. Stratigraphic column of the Western Mecsek uranium ore deposit (modified after Barabás 2013) showing the red arrow is uranium ore zone and blue frame indicates grey sandstone, where has been sampled.

Sandstone, Kővágótőttős Sandstone, Cserkút Sandstone, and Tótvár Sandstone. Early Triassic Jakabhegy Sandstone Formation and Patacs Siltstone formations are characterized by red sandstone, fine-grained red siltstone, and green claystone.

3. Samples and Methods

3.1. Sample Collection Sites

Eight rock specimens were selected from drill core samples retrieved from borehole WHE-I/2, located in the vicinity of a closed uranium mine, approximately 15 km west of Pécs city. These samples were obtained from depths ranging between 832 m and 907 m within a strongly reducing zone, which extended into the lower depth interval of the Kővágótöttös Sandstone in the KSF. The samples were labeled WH2, derived from the borehole's name, WHE-I/2. These rocks comprise a mixture of siliciclastic and carbonate materials (see Fig. 3).

3.2. Analytical and Experimental Methods

The identification of mineral inclusions within the samples involved employing X-ray powder diffraction (XRPD) utilizing a BRUKER D8 ADVANCE instrument with Cu-Kα radiation at 40 kV and 40 mA. Elemental compositions of selected minerals were determined through Wavelength Dispersive X-ray Fluorescence (WD-XRF) analysis conducted on a RIGAKU Supermini instrument with a Pd source, operating at 50 kV and 4 mA. The mineralogical composition was quantified using the Rietveld refinement method applied to XRPD data, employing the Reference Intensity Ratio (RIR) approach to determine the

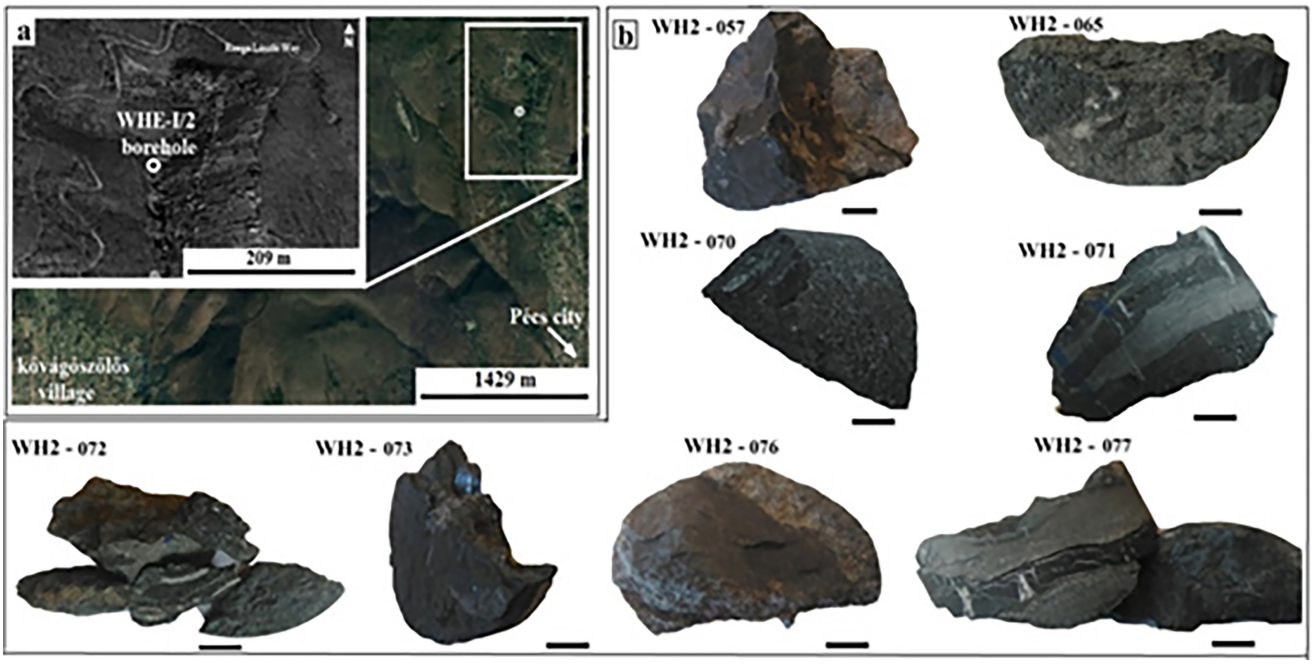

Fig. 3. Overview map of the closed uranium mining area in Western Mecsek showing the drill well WH2 (a) and collected hand specimens of the drill core samples (b). Scale for rock fragments – 1 cm.

relative abundance of each mineral phase.

For imaging purposes in both incident normal and fluorescence light modes to evaluate organic petrology and mineralogy, a Zeiss AxioImager (A2m) microscope was utilized. Light detection was facilitated by a monochrome camera (AxioCam MRc5) along with the AxioVision Rel. 4.8 software by Carl Zeiss MicroImaging GmbH, enabling examination in both transmitted and reflected light modes. Reflected-light organic petrography was carried out using a Zeiss UMSP 50 microscope equipped with 50X oil immersion lenses.

Elemental analysis of minerals such as sulfide minerals (pyrites, galena, sphalerite) and minor uranium ore minerals, as well as determination of sulfur, chlorine, and phosphorous content in the organic phase, was performed using electron microprobe analysis (EMPA) with backscattered electron (BSE) imaging, energy dispersive spectroscopy (EDS), and X-ray mapping on a JEOL SXA 8600 Super probe operated at 20 keV and 20 mA.

Total organic carbon (TOC %) content was determined using an organic elemental analyzer (OEA, ELTRA's CS-2000) on carbonate-free samples, after removing inorganic carbonate minerals with 10% chloric acid.

The experimental procedure followed a sequential extraction technique conducted in three distinct stages, based on the method of Lakatos et al. (1997); Varshal et al. (2000); Mukherjee and Borthakur, (2003); Henrique-Pinto et al. (2015); Junussov et al. (2018); and Junussov et al. (2019). Initially, the extraction of humic acid was performed using potassium hydroxide (45 ml of 1M KOH, with samples, heating for 2 hours in a water bath set at 70°C) from 5 grams of powdered samples (63 μm) in the first step. Subsequently, in the second stage, hydrochloric acid (22.5 ml of 37% HCl, heating with samples at 60°C for 1 hour in a water bath) was employed to extract carbonates, sulfide, sulfate, and iron oxide. Finally, the third stage involved the use of aqua regia (68% HNO_3 + 37% HCl, 1:3; heating with samples in a water bath at 80°C for 30 minutes) to extract iron sulfide.

Gold (Ag, Pt and Pd) concentration in both bulk and sequentially separated liquid extracts from all three stages was analyzed using inductively coupled plasma-optical emission spectroscopy (ICP-OES) on a 720 ES instrument by VAR-IAN Inc.

All analytical and experimental methods, along with other procedures, were conducted at the University of Miskolc, Hungary.

4. Results

4.1. Mineralogy and Elemental Compositions

As per X-ray powder diffraction (XRPD) data, quartz makes up to 25 weight percent, while feldspar minerals collectively contribute 20.2 weight percent, with microcline accounting for 12 percent and albite 8.2 percent. Carbonate minerals vary from 7.7 percent for ankerite to 19.5 percent for dolomite. Clay minerals constitute 14.3 percent, including 13 percent illite, 0.7 percent smectite, and 0.6 percent kaolinite. Traces of muscovite and titanomagnetite are also observed.

Chemical analyses confirm the presence of major felsic rock-forming minerals containing elements such as Si, Al, Na, K, Mg, Mn, and Ca, with quartz, potassium, and sodium feldspar minerals ranging from 2 to 62 percent, and carbonate minerals. Minor elements like Ti (with an average of 0.28 percent) and P (with an average of 0.09 percent) form compounds of titanium-oxide and phosphate minerals (shown in Table 1).

4.2. Organic Petrology

The sandstone samples exhibit five distinct types of organic matter, which are consistently present across all samples (Fig. 4 a and e). These include solid bitumens of non-fluorescing pyrobitumen PB, filamentous non-fluorescing B1 and fluorescing bitumen B2; and infilling voids between cells of primary (telinite) vitrinite V1 and reworked vitrinite V2.

Pyrobitumen PB is observed as dark brown to grayish-colored material in reflected normal light, filling fractures and voids in quartz. It is often observed as discrete dots or filaments, with a homogenous texture and grey color in thicker veins and voids.

Table 1. XRD and XRF results of eight samples

	Samples							
Contents	WH2-57	WH2- 65	WH2-70	WH2-71	WH2-72	WH2-73	WH2-76	WH2-77
Minerals	*Mineralogical composition (unit, wt%)*							
Quartz	35.2	34.9	44	4.5	10.2	23	31.6	14.5
Muscovite	16.2	-	-	-	-	-	-	-
Albite	9.9	12.1	11.6	-	6.6	11.2	11	3.3
Ankerite	8.3	2.3	3	19.5	13.6	1.4	0.7	6.6
Mg-siderite	-	-	-	-	-	3.7	-	-
Mn-siderite	-	-	-	-	-	1.7	-	-
Smectite	0.3	1.2	2	-	-	1.6	1	-
Kaolinite	-	1	-	-	-	1.9	0.5	1.5
Illilte	6	19.7	10.5	-	5	25.3	22.7	10.9
Dolomite	19.6	2.8	4	41.5	26.3	10.2	4.1	47.6
Microcline	-	16.6	15.8	-	16.8	16	16.3	9.4
Titano-magnetite	0.5	1.8	2.1	-	-	-	0.3	-
Chlorine	-	-	-	-	-	-	4.7	-
Elements	*Chemical composition (unit, wt%)*							
SiO_2	57.8	63.3	65.3	1.2	13.8	51.7	62.1	30.3
Al_2O_3	8.9	16.6	11.3	0.2	2.7	14.5	16.8	5.9
MgO	5.34	1.72	1.4	5.31	4.88	3.59	2.08	10.28
CaO	10.4	1.53	1.45	13.9	10.1	4.06	1.06	17.2
Na_2O	1.15	1.26	1.27	0.1	0.2	0.87	1.22	0.45
K_2O	3.88	5.67	4.06	0.13	0.99	5.26	6.2	2.66
Fe_2O_3	2.26	1.31	6.71	11.1	19.5	6.24	2.24	3.43
MnO	0.436	0.047	0.042	0.269	0.128	0.155	0.038	0.36
TiO_2	0.205	0.418	0.179	0.009	0.124	0.584	0.478	0.258
P_2O_5	0.051	0.058	0.04	0.059	0.09	0.097	0.259	0.074

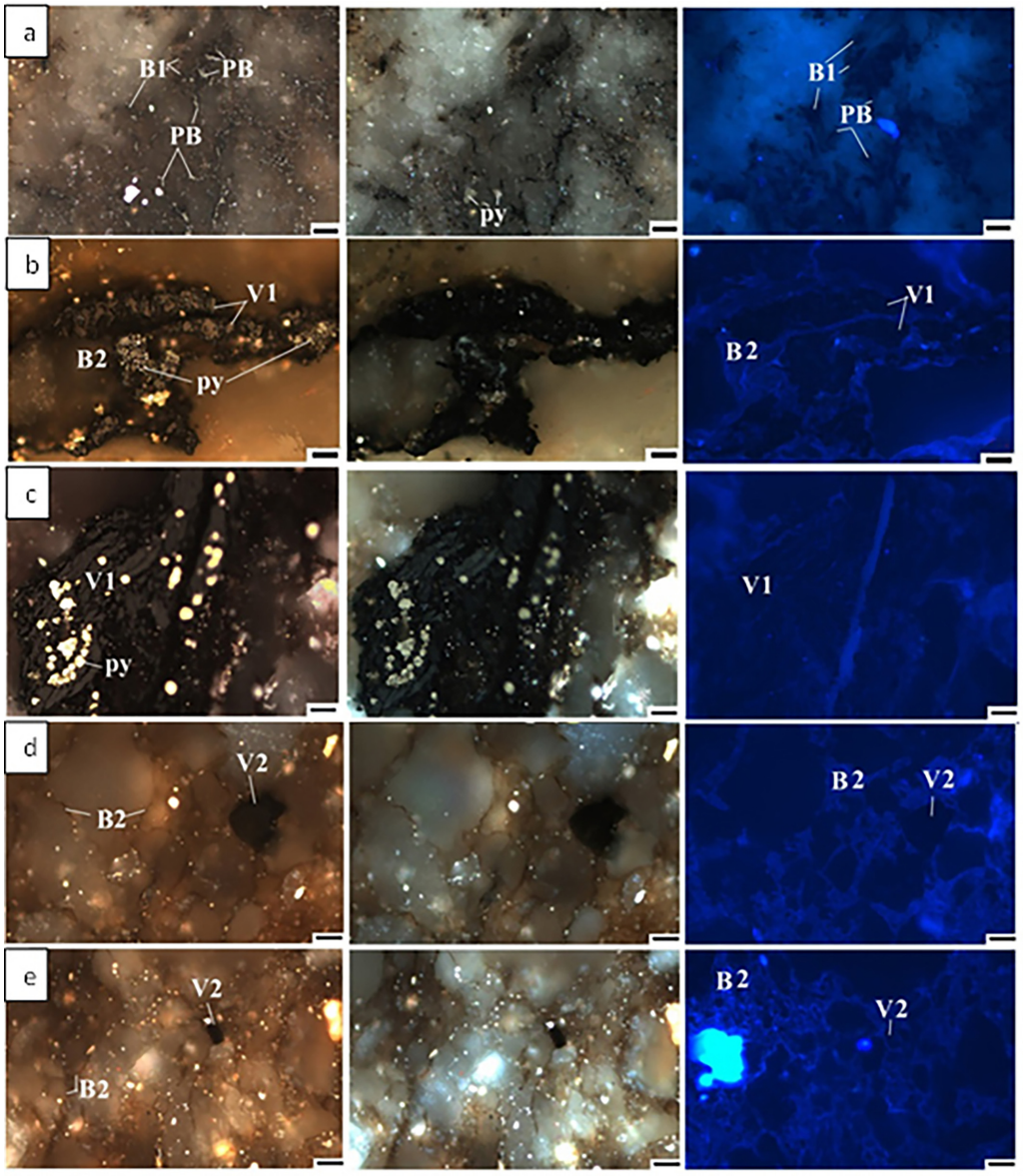

Fig. 4. Photomicrographs (in oil immersion) of organic matter from samples WH2-57, WH2-65, WH2-77: a) Pyrobitumen PB showing the small dots of non-fluorescing and homogenous grey color void fillings; (b and c) Solid bitumen B2 filling of brownish veins with slightly fluorescing bitumen in between the vitrinite particles and non-fluorescing solid bitumen B1 in between telinite cells of the vitrinite V1 and framboidal pyrite (py); (d and e) fine-grained fragments of reworked vitrinite V2 occurred as telinite and slightly fluorescing solid bitumen B2 (intense whitish fluorescence displays no uranium mineral. Legend: The PPL on the left side, XPL in the central column, and fluorescent light illumination on the right side. Scale – 10 μm.

Non-fluorescing solid bitumen B1 is present in the voids between cells or cracks of primary (telinite) vitrinite V1. It typically presents as dark brownish material and lacks fluorescence under ultraviolet illumination.

Filamentous fluorescing solid bitumen B2 occurs as fillings between rock particles, ranging from thin to large fractures and voids in quartz. It exhibits a slightly fluorescing property and appears as dark brownish filamentous material.

Primary (telinite) vitrinite V1 is found within fractures of dolomites and is characterized by its larger size compared to V2, ranging from 10 to 50 microns. It is associated with the fluorescing bitumen B2.

Reworked vitrinite V2 is smaller in size compared to V1, ranging from 10 to 50 microns. It has an angular shape and is typically associated with fluorescing bitumen B2.

The distribution of these organic matter types varies with

depth, with pyrobitumen (PB), coarse-grained vitrinite (V1), and non-fluorescing solid bitumen (B1) increasing relatively with depth, while B2 and V2 decrease. The detailed elemental contents of the organic matter obtained from EPMA are reported separately.

4.3. Microprobe Analysis for Grains of Organic Matter and Ore Minerals

During microprobe analysis (Fig. 5 a and f), we investigated vitrinite particles (referred to as V1), focusing particularly on those found as inclusions within diagenetic pyrite crystals and two other types of veined bitumen. However, due to their delicate microtextures, identifying individual elements in the latter two types proved challenging, as noted in previous studies (Belin 1994; Cardott et al., 2015). The diagenetic pyrite growths within the vitrinite particles displayed globular or framboidal structures, sometimes polyframboidal, as observed in earlier research (Hámor 1994).

A direct determination of total organic carbon in the vitrinite particles was undertaken. In Fig. 5 a-d, a BSE image was selected for X-ray mapping analysis, revealing

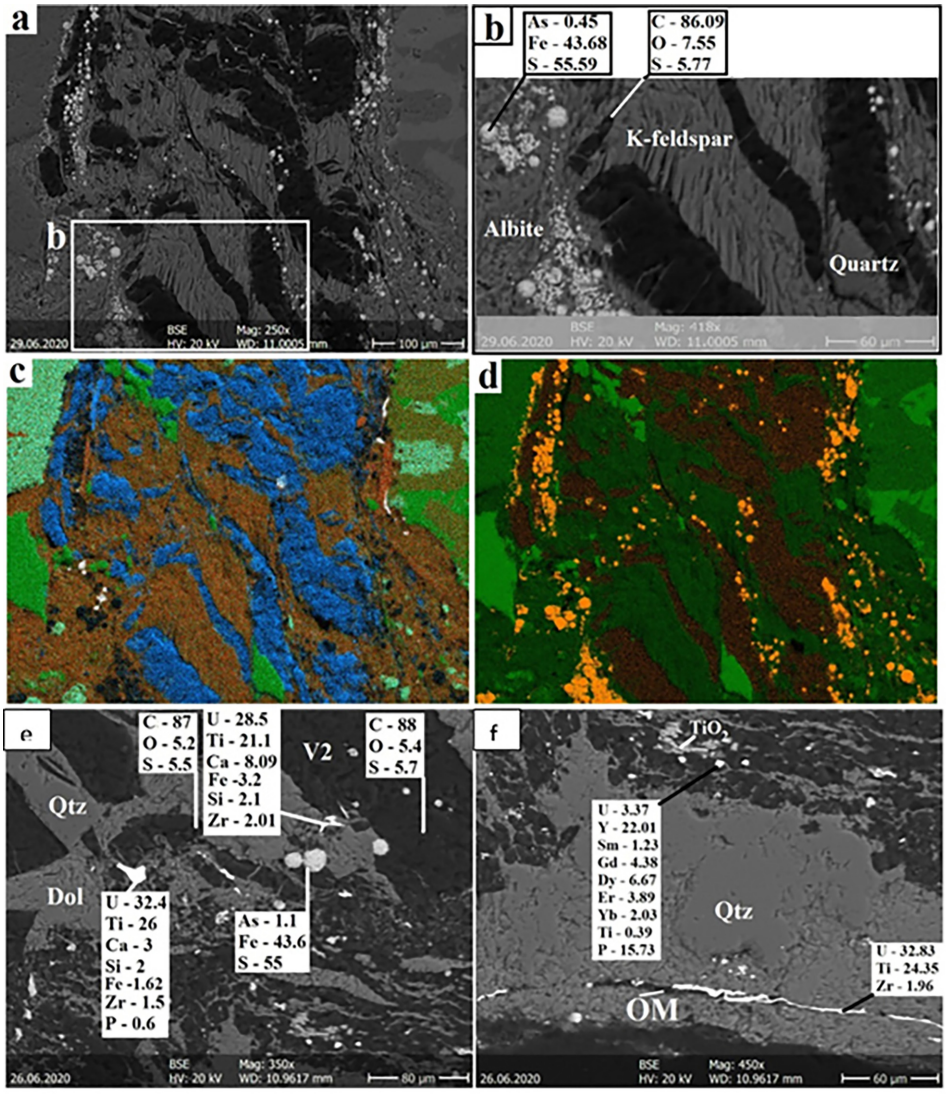

Fig. 5. EMPA-EDS X-Ray map of organic matter and framboidal pyrites from samples WH2-76 and WH2-70: BSE images (a and b) and X-Ray mapping images (c and d) – organic matter (shown in blue) and rock matrixes (denoted albite in cyan, quartz in green, K-feldspar in brown (and dark green), and titanium oxide in white, sulfur content in dark orange, and pyrite in light orange with surrounding silicates; e) organic matter and subhedral Ti-Ca-rich coffinite; and f) subhedral U and REE-bearing phosphorus minerals and needle-like Ti-rich uraninite within organic matter in the dolomite veins with quartz grains.

elemental composition values of 86 wt% carbon and 5.7 wt% organic sulfur. Other authors, Harrison (1991) and Ward & Gurba (1998) successfully measured the amount of organic sulfur in individual maceral grains of bituminous coals. Furthermore, chlorine was detected in the vitrinite of sample WH2-65, ranging from 0.05 to 0.10 wt%. Various greyish-white spots within the clay matrix and at the periphery of vitrinites indicated the presence of individual, framboidal, and polyframboidal pyrite crystals (10 μm), containing an arsenic content of 0.4 wt%. The EMPA X-ray map revealed the presence of vitrinites in blue, accompanied by pyrite (dark blue) within microcline grains (brown), and surrounded by other mineral formations. Organic sulfur was exclusively linked with the vitrinite, manifesting as a dark orange color. Conversely, sulfur originating from pyrites was dispersed both along and within the vitrinite matrix and within the clay grains, visualized as a light orange color.

Three distinct phases of uranium ores were identified within the samples: uraninite (pitchblende), coffinite, and U-REE-bearing phosphorus minerals (See Fig. 5 e and f). Uraninite was found in veinlet or needle-like formations within fractures alongside dolomite and quartz, closely associated with vitrinite. The size of these needle-like uraninite structures varied from 10 μm to over 100 μm, while coffinite measured approximately 20 μm in size. Both minerals exhibited significant concentrations of titanium (up to 26 wt%). Calcium (3-8 wt%), silicon (2 wt%), phosphorus (up to 0.6 wt%, partially absent), and zirconium (up to 2 wt%) elements were notably enriched in coffinite. Although uraninite (UO2) predominated as the most abundant U mineral, its stoichiometric formula was slightly altered due to titanium and zirconium enrichment. Pure coffinite was not observed in the samples. The third type of uranium mineral identified was a low-grade U-bearing phosphorus mineral, characterized by a uranium concentration of up to 3.4 wt%. This type was finely dispersed in particles of vitrinite and clay minerals, exhibiting a diameter of 3 μm. Noteworthy rare earth elements found in the uranium minerals included yttrium (22 wt%), dysprosium (6.7 wt%), gadolinium (4.4 wt%), erbium (3.9 wt%), ytterbium (2 wt%), and samarium (1.3 wt%). Accessory minerals, such as monazite (20-30 μm) and zircon (12 μm), were detected in trace amounts associated with clay minerals and DOM of the samples. No free grains of precious metals were detected in the organic matter particles.

Table 2. TOC (total organic carbon) content of eight samples

Samples	Depth (m)	TOC % value
WH2-57	831.4	0.5
WH2-65	847.6	0.9
WH2-70	865.9	0.8
WH2-71	870	1.1
WH2-72	870.5	1
WH2-73	883.3	0.6
WH2-76	895.6	1
WH2-77	907.5	0.7

4.4. TOC and Elemental (H, N, S) Analysis

The Total Organic Carbon (TOC %) in the eight samples ranges from 0.5 wt% to 1 wt%, averaging at 0.83 wt%. Sample WH2-57 has the lowest TOC % at 0.5 wt%. The concentration of organic matter increases gradually with depth, with sample WH2-70 having a mean TOC value of 0.8% and the highest TOC content of 1.1% found in sample WH2-71.

Hydrogen, nitrogen, and sulfur were assessed using the organic elemental analyzer. Hydrogen content ranges from 0.23 wt% in sample WH2-57 to 1.74 wt% in sample WH2-77, averaging at 0.76 wt%. Nitrogen levels vary from 0.025 wt% in sample WH2-57 to 0.15 wt% in sample WH2-77, with an average of 0.073 wt%. Total sulfur content ranges from 0.16 wt% (sample WH2-57) to 5.81 wt% (sample WH2-77), with an average value of 2.79 wt% (Table 2).

4.5. Experimental Results

Three sequential extraction steps were employed to separate gold and silver from the soluble organic matter within the samples, focusing on two exchangeable fractions bound to the organic matter and sulfide minerals.

Optical and electron microscopy did not reveal free gold grains within either the organic matter or sulfide minerals. Despite this, the extraction experiments successfully isolated gold from both the organic fraction and the handpicked arsenian pyrite-bearing minerals. In addition to gold, the organic fraction also contained silver, but no platinum metals were detected, indicating that both gold and silver

Table 3. Results of extracted metals from selected samples in the three stages

Samples	Three steps with chemicals and elements values (unit, ppm)							
	I step (KOH) / DOM							
	Au	Ag	As	Fe	Cu	Zn	Pb	Sb
WH2-057	2.28	0.11	2.2	1.8	0.03	0.02	-	-
WH2-073	1.89	0.01	5.3	0.1	0.36	0.36	-	0.05
WH2-077	3.28	0.07	3.3	0.3	0.07	0.02	-	-
Average (unit, ppm)	2.48	0.06	3.6	0.73	0.15	0.13	-	0.025
Samples	II stage (HCl) / Sulfide minerals							
	Au	Ag	As	Fe	Cu	Zn	Pb	Sb
WH2-057	0.2	0.19	2.9	749	0.05	0.4	0.4	-
WH2-073	0.44	0.18	7.1	1041	0.55	7.1	5.6	-
WH2-077	0.63	0.15	6.7	639	0.75	0.5	29	-
Average (unit, ppm)	0.42	0.17	5.56	809	0.45	2.6	11.6	-
Samples	III stage (Agua regia) / Residual materials							
	Au	Ag	As	Fe	Cu	Zn	Pb	Sb
WH2-057	-	1.19	84	393	0.4	0.6	0.3	0.33
WH2-073	-	0.89	61	1045	2.5	18	2.1	0.06
WH2-077	-	0.78	37.5	1136	2.8	1.2	3.4	0.07
Average (unit, ppm)	-	0.95	60.8	858	1.9	6.6	1.9	0.15

Note: TOC (%) concentration reaches 0.5 % in WH2-057; 0.6% in WH2-0.6 and 0.7% in WH2-0.7%

are finely dispersed within the organic matrix.

Gold and silver concentrations were quantified using ICP-OES, as shown in Table 3, for the two different phases of the soluble organic fractions and sulfide minerals from three samples.

In the first stage of sequential fractioning, the total amount of dissolved gold was found to be 7.45 ppm (2.48 g/t on average), along with a silver concentration of 0.19 ppm. Other elements were present in much smaller quantities in this stage.

During the second sequential stage, the high concentration of hydrogen chloride-initiated leaching, resulting in a total amount of 1.27 ppm gold (0.42 g/t on average) and 0.52 ppm silver. Additionally, higher amounts of iron (1041 ppm) and lead (up to 29 ppm) were detected, while arsenic remained in smaller quantities.

In the third sequestration stage, aqua regia completely dissolved the remaining metals, and sulfide minerals. In the dissolved material, arsenic (up to 84 ppm), iron (1136 ppm), copper (2.8 ppm), zinc (18 ppm), and antimony (0.3 ppm) were observed, with an elevated total concentration of silver up to 2.86 ppm, likely originating from sulfide minerals. However, gold was not detected.

The analysis highlighted significant differences in gold and silver distributions between the organic matter and sulfide minerals. Notably, a greater proportion of gold was associated with the organic matter (7.45 ppm) compared to the sulfide minerals (1.27 ppm). Conversely, silver concentrations were higher in the sulfide minerals (3.38 ppm) than in the organic matter (0.19 ppm). Among the samples, WH2-77 exhibited the highest gold content, whereas WH2-57 had the highest silver concentration.

5. Discussion

5.1. Mechanisms of Organic Matter and Gold Occurrence

The investigation of organic matter in conjunction with two vitrinite types and various solid bitumen types has also been reported by Junussov et al. (2024). Vitrinite of organic matter in the samples is the dominant maceral present.

These outcomes indicate a probable humic acid source for the terrestrial organic matter, likely originating from a fluvial environment. Additionally, geochemical analysis indicates the presence of sulfur-rich polycyclic hetero-aromatic hydrocarbons within the organic matter. Total organic carbon (TOC) content ranges from 0.5% to 1.1%. The same samples within organic matter show high thermal maturity, with a random vitrinite reflectance (Ro) of 2.25% (Junussov et al., 2024). This indicates significant thermal alteration and evolution of the organic matter over time.

Gold is found in varying concentrations within the organic matter of the Permian-Early Triassic Sandstones in the Western Mecsek Mountains, which is situated in the same region as the Permian KSF with elevated uranium content (Barabás & Konrád, 2000). As per (Szalay, 1954), uranium is believed to originate from the granite of the Mórágy complex. It is plausible that gold also originates from the granite complex, alongside uranium. The enrichment of organic-rich sequences with gold likely occurs through processes involving surface and groundwater or hydrothermal leaching of the granitoid complex's underlying and denuded surfaces.

Organic matter demonstrates a high level of maturation, indicating a progression towards the semi-anthracite to anthracite stage. This is supported by the presence of highly reflective and uniform pyrobitumen. Furthermore, the reworked vitrinite V2 particles display increased reflectivity, particularly evident in sporinite. Telinite V1 is notably abundant in the lower zone, beginning at a depth of 847.6 meters. Additionally, small-sized angular vitro-detrinite is prevalent in samples WH2-072, WH2-076, and WH2-077. Within the organic matter, it is apparent that a portion of the solid bitumen has undergone significant thermal alteration, further contributing to the maturation process. The distinct migration patterns observed in the dark brown solid bitumen and pyrobitumen, alongside the accumulation of uranium ore near vitrinite and pyrobitumen particles, provide compelling evidence for the influence of epigenetic hydrothermal processes. Rojkovic et al., (1992) described the hydrothermal alteration of the organic matter, attributing it to the influence of radioactive α decay during uranium (U) mineralization in Permian organic matter. Similar alterations of organic matter are reported in studies by (Sýkorová et al., 2016) and (Machovič et al., 2021) in uranium deposits, where increased thermal maturity, aro-matization, and decreased H/C atomic ratio are observed. Hydrothermal deposits of gold and base metals are discussed by (Parnel et al., 1993). However, we propose that the thermal alteration of organic matter in our case results from a combination of hydrothermal alteration and radioactive decay. Desiccation patterns observed in vitrinite grain cracks and the porous texture of telinite, along with lower reflectivity fields in the particle, suggest the influence of α decay. Nevertheless, radiation-induced haloes in the organic matter are rare.

The detection of chlorine within primary vitrinite V1 suggests the influence of Cl-rich groundwater during early diagenesis, as discussed by Caswell et al. (1984a) and (Caswell, et al., 1984b).

The hydrothermal effect is substantiated by several factors: (1) the presence of pyrobitumen associated with gold in the organic matter; (2) enrichments of sulfur and chlorine contents in the organic matter; and (3) transformation of framboidal pyrite crystal growth in vitrinite to recrystallized euhedral pyrite with arsenic content. The solid bitumen B1 is believed to have undergone migration facilitated by hydrothermal fluids, moving from regions of higher temperatures towards lower temperatures, eventually reaching larger voids within the host rock. This migration process facilitated the aggregation of metal-organic complexes and gold. PB migrated through extremely thin fractures and voids within the dolomite, as well as between quartz grains of the host rock. It is preserved in the form of tiny, thin-filling structures within the dolomite and quartz veins, showing no fluorescence intensity. However, in pore fillings, its homogenous nature is evident. The presence of a thin membrane adhering to mineral grains suggests that the bitumen was precipitated as an immiscible phase within the hydrothermal fluid (Simoneit 1994, 2000, 2018). Subsequently, it flowed along the walls of the veins, transitioning into this form of PB. Furthermore, the vitrinite appears in the form of large telinite and desmocollinite, which are relatively common in the lower zone. Additionally, small-sized angular vitrinite is observed in parts of the coarser arkosic siltstone in WH2-057, WH2-072, and WH2-076. The large vitrinite particles containing telinite and desmocollinite V1 often harbor framboidal and polyframboidal early diagenetic pyrite. These pyrite formations are of microbial origin, where pyrite crystals grow from the edge towards the core of the pyritization

area. The formation of such framboidal pyrite in organic matter has been attributed to the early diagenesis of coalified plant tissues, as described by Hámor (1994). Additionally, studies by Berner (1969) and Raiswell (1982) have highlighted that pyrite formation is a result of the decomposition of the most readily metabolized organic matter through bacterial sulfate reduction. Pyrite formation can occur under various sedimentary microenvironmental conditions, as further detailed by Hámor (1994) and Nayak et al. (2008). The vitrinite particles in our samples exhibit a carbon content of 86 wt% and total sulfur ranging from 5-6 wt%, forming a sulfur-rich organic matter. Thiophenic compounds found within these particles are known to remain thermally stable in hydrothermal fluids up to temperatures of 250°C, as evidenced by the research of Giordano (2000).

5.2. Role of Organic Matter in Gold Migration and Entrapment

The analytical results obtained by ICP-OES for organic matter exhibiting high-grade gold concentrations provide insights into the close association between metals and various organic components such as vitrinite, and solid bitumen. This association suggests that the organic matter has played a crucial role in the migration and entrapment of gold. The presence of a network of veins and veinlets filled with vitrinite and solid bitumen, along with the occurrence of organic matter inclusions in detrital and authigenic quartz grains, provides compelling evidence supporting the hypothesis that vitrinite and solid bitumen originated from a mobile precursor, likely liquid hydrocarbons. These findings indicate that uranium, gold, silver, and thorium are enriched relative to their concentrations in the organic-rich sediments, with uranium and gold particularly exhibiting notable enrichment. Földessy (1997) confirmed gold preferentially concentrates in organic-rich layers, enriched by surface and groundwater or hydrothermal leaching of the underlying granitoid complex. Organic matter is enriched in gold, likely due to its ability to bind metals to aromatic acids and form colloidal phases absorbing metals from water solutions (Giordano, 1994; Wood, 1996; Seredin and Finkelman, 2008). Gold mineralization likely occurred during infiltration circulation of sulfur-rich groundwater, enriched in gold and silver, heated by radioactive decay of uranium ores, and increasing geothermal gradient related to burial. Gold migrated with liquid bitumen in ore-forming solutions in sulfur-rich groundwater fluids, precipitating within dolomite minerals and intergranular quartz. Seredin (2007) and Seredin and Finkelman (2008) explained that ionic gold concentration in coal materials decreases with decreasing absorption capacity of organic matter in groundwater solutions with increasing coal rank, suggesting metal-organic complexes form during early diagenesis. The gold accumulation in the Western Mecsek implies finely dispersed gold mineralization within organic matter during bituminization at a Raman-estimated temperature above 144.5±30ºC (Junussov, 2022). As Baruah et al. (1998) mentioned, gold is bonded to the organic matrix with sulfur-rich heterocyclic aromatic hydrocarbons of the coaly-type organic matter, possibly as thiosulfate complexes.

The presence of needle-like or veined uranium-titanium ore minerals observed within the organic matter and dolomite veins, alongside subhedral uranium-phosphate ore minerals found in fractured autochthonous vitrinite particle V1 matrix and between quartz grains, suggests a paragenetic association of uranium with solid bitumen. Additionally, rare earth elements (REE) are enriched within the V1 matrix as a phosphate phase, with finely dispersed monazite exhibiting high uranium content. This interpretation is supported by previous research conducted by Barabás and Konrád (2000), who investigated uranium mineralization and indicated that uranium mineralization in the form of nasturan or pitchblende U_3O_8 occurs at hydrothermal temperatures of up to 200ºC. They proposed that uranium leaches out from the uranium-bearing granite and migrates with subsurface waters. Furthermore, Barabás (2013) evaluated that the average uranium concentration in the presumed source-rock granite ranges from 7 to 10 g/t, with total REE concentrations ranging from 52 ppm to 290 ppm.

Primary syngenetic model in Fig. 6 illustrates the accumulation of uranium ore deposit, surface waters in the fluvial system (based on Szalay, 1954; Fehn et al., 1978; Barabás, J. (1979) Santbrd, 1994; Barabás and Konrád, 2000; and Raffensperger and Garven, 1995), along with changes in the redox conditions of the basement and subsurface groundwater flow, favoured the precipitation of uranium, often associated with Cu, V, and Cr. Uranium precipitated from waters percolating laterally and downwards,

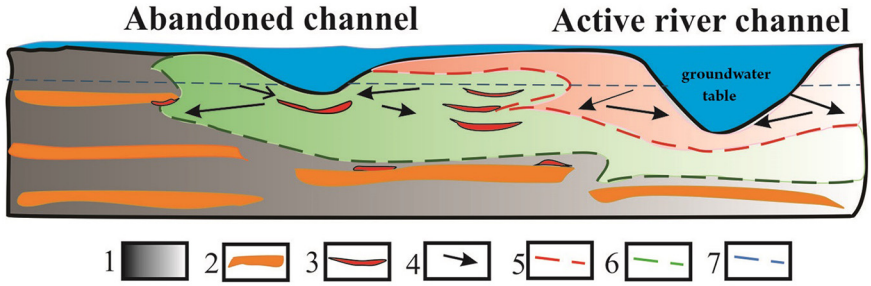

Fig. 6. Primary syngenetic model of the accumulation of uranium ore deposit in Western Mecsek. (modified after (Barabás, 2013), and (Virágh and Vincze, 1967) Legend: 1) Fluvial floodplain sediment; 2) Peat-forming sediments; 3) Ore accumulation lenses; 4) Sub-surface water flow; 5) A border between oxidized and intermediate rock types (red and green sandstone); 6) A border between intermediate and reductive rocks (green and grey sandstone); 7) Mean groundwater level.

with optimal conditions found in abandoned channels, oxbows, ox-bow lakes, and swamps where grey sediments rich in organic matter accumulated. Conversely, oxidizing conditions in the central basin led to the development of red sandstones. Commercial-grade uranium ore formed in the green sandstone sequence between these zones. However, uranium dissolution occurred in some areas due to oxidation processes. The dissolved uranium adsorbed on the surface or in the vicinity of decomposing organic matter, forming metal-organic colloids. Hydrodynamics facilitated the entrapment of uranium in reducing sediments, leading to gradual enrichment and the formation of commercial uranium concentrations. Studies by Santbrd (1994) and others have highlighted the strong reductive properties of organic matter, suggesting its role in protecting the ore from oxidation and destruction. Additionally, it is proposed that uranium concentrates near organic matter accumulations either through gravity-driven groundwater flow or large-scale thermal convection cells initiated by the release of accumulated heat through fracture zones in radioactive granites (Raffensperger and Garven, 1995; Fehn et al., 1978).

Electron microscopy results revealed that the fracture-filling needle-like uranium ore minerals in dolomite veins were enriched in titanium. Other subhedral forms of the ore minerals contained phosphorus and titanium, with small quantities of zinc. The high concentrations of phosphorus and titanium suggest that uranium ore minerals mobilized with solutions containing elevated levels of dolomite and later precipitated together in accumulation zones. The uranium accumulation in the Late Permian KSF is closely linked to the primary weathering processes of Late Carboniferous magmatic rocks and epigenetic dissolution from the underlying granitoid complex (Virágh and Vincze, 1967). Uranium easily migrates in surface and subsurface waters and precipitates in reducing environments or on highly adsorbing materials like organic matter, clay minerals, and iron oxides, typically in intermediate transition zones between oxidizing and reducing environments.

The semi-arid climate of the palaeogeographic setting, with lush vegetation in geomorphological depression zones, creates conditions favourable for uranium adsorption onto organic matter under reductive conditions. In Western Mecsek, sandstone-type uranium accumulation occurs in sedimentary sequences where flat slopes of alluvial rocks build up fine-grained sandstone, clay, and siltstone lenses. The ore formation is associated with local accumulation anomalies of organic matter in fluvial sedimentation.

6. Conclusion

Based on extensive research data from the Western Mecsek uranium ore deposit, the following insights into the roles of organic matter in gold mineralization can be proposed: 1). Organic matter derived from coal exhibits a humic acid organic structure enriched in sulfur-containing heterocyclic aromatic hydrocarbons; 2). Organic matter predominantly occurs as primary vitrinite, pyrobitumen, and brownish solid bitumen, precipitating within fractures in dolomite and quartz of the host rock. Secondary reworked vitrinite forms through bitumen activity; 3). Gold enrichments are concentrated in organic matter-rich reducing zones, particularly within pyrobitumen; 4). Organic matter actively participates in gold mineralization by facilitating

the migration of gold and hydrocarbons through fluid processes. Gold becomes trapped in heteroaromatic fractions of pyrobitumen, with dissolved organic matter mediating absorption and entrapment in metal-organic complexes within small veins and voids. 5). Organic matter facilitates the migration of dissolved uranium, leading to the precipitation of uranium oxides in dolomite veins and dispersed subhedral uranium phosphate minerals in the clay matrix. 6). Organic matter likely acts as a concentrator, transporter, and preserver of gold, as well as uranium and sulfur within the deposit.

These insights, combined with an understanding of the role of organic matter in gold occurrence and the use of sequential extraction and ICP-OES methods, could serve as valuable tools for assessing the exploration potential of gold within the deposit and other types of organic-rich sedimentary gold ore deposits.

Acknowledgment

Special thanks are extended to Prof. Dr. F. Mádai and M. Hámorne-Vidó for their valuable comments and discussions. Dr. Kristály F. is acknowledged for X-ray powder diffraction (XRPD) and electron microprobe analysis (EMPA), while Dr. Krisztián F. conducted Raman measurements. Dr. Gábor M., Dr. Olivér B., Dr. Vanyorek L., and Ádám P. provided the assistance with ICP-OES, FTIR, OEA measurements, and chemical experiments. Special appreciation is extended to D. Debus, F. Móricz, J. Richards, and M. Leskó for their contributions to the laboratory experiments that supported the preparation of this paper.

Funding Declaration

The authors acknowledge the financial support from the Social Policy Grant (064.01.00 SPG), Nazarbayev University.

Reference

Barabás, A. (1956) Permian formation of Mecsek. The dissertation. (A mecseki perm-idõszaki képzõdmények - Kandidátusi Értekezés - MÁFI – Könyvtár, in Hungarian). p.94.

Barabás, A. (1979) Geological conditions of the Permian and tasks of surface geological investigations at the Mecsek ore deposit). Föld Közl 109(3-4), p.357-365 (in Hungarian with English abstract).

Barabás, A., Konrád, Gy (eds.)., (2000) Zárójelentés a magyarországi uránérc-kutatásról és a nyu-gat-mecseki uránérc-bányászatról. Kézirat, MECSEKÉRC Zrt. Földtani Adattár. (Final report of the uranium exploration of Hungary and Western Mecsek uranium ore mining. Manuscript in Hungarian)

Barabás. A. (2013) Hasadó anyagok. (Pál-Molnár E. and Bíró L. eds.) In: Szilárd ásványi anyagok Magyarországon. (Fission mineral resources. Solid mineral resources of Hungary; in Hungarian), Geolitera publisher, SzTE TTIK Földrajzi és Földtani Tanszékcsoport, Szeged, p.89-121.

Baruah, M.K., Kotoky, P. and Borah, G.C. (1998) Gold in High Sulphur Indian Coals. Fuel, v.77(15), p.1867-1868.

Berner, R.A. (1969) Migration of iron and sulfur within anaerobic sediments during early diagenesis. Am. J. Sci., v.267, p.19-42.

Belin. S. (1994) Backscattered electron imaging applied to source rock sedimentology: a comparison with conventional methods in organic petrology. Bulletin Des Centres De Recherches Exploration-Production, v.18 Special Publication, p.165-187.

Cardott, B.J., Landis, C.R. and Curtis, M.E. (2015) Post-oil solid bitumen network in the Woodford Shale USA—a potential primary migration pathway. Int. J. Coal Geol., v.139, p.106-113. doi: 10.1016/j.coal.2014.08.012

Caswell, S.A., Holmes I.F. and Spears D.A. (1984a) Total chlorine in coal seam profiles from the South Stafford-shire (Cannock) coalfield. Fuel, v.63, p.782-787. doi: 10.1016/0016-2361(84)90068-1

Caswell, S.A., Holmes I.F. and Spears D.A. (1984b) Water-soluble chlorine and associated major cations from the coal and mudrocks of the Cannock and North Staffordshire coalfields. Fuel, v.63, p.774-781. doi: 10.1016/0016-2361(84)90067-X

Emsbo, P. and Koenig, A. (2007) Transport of Au in petroleum: Evidence from the northern Carlin Trend Nevada [abs]: Digging Deeper Biennial SGA Meeting 9th Dublin Society for Geology Applied to Mineral Deposits Proceedings, p.695-698.

Fazekas, Via. (1987) A mecseki perm és alsótriász korú törmelékes formációk ásványos összetétele. Földtani Közlöny, Butt, of the Hungarian Geol. Soc., v.117, p.11-30.

Fehn, U., Cathles L.M. and Holland H.D. (1978) Hydrothermal convection and uranium deposits in abnormally radioactive plutons. Econ. Geol., v.73, p.1556-1566. doi: 10.2113/gsecongeo.73.8.1556

Földessy, J. (1997) Exploration potential of the Western Mecsek area. Report of the Rotaqua Kft. Kővágószőllős, p.11.

Földessy, J. (1998) Geological Report: Diagnostic sampling of the formations of the Western Mecsek mountains. Budapest, p.8.

Fodor, L., Jelen, B., Márton, E., Skaberne, D. and Vrabec, M. (1998). Miocene-Pliocene tectonic evolution of the Slovenian Periadriatic Line and surrounding area - implication for Alpine-Carpathian extrusion models. Tectonics, v.17, p.690-709. http://dx.doi.org/10.1029/98TC01605

Giordano, T.H. (1994) Metal transport in ore fluids by organic ligand complexation in Pitman ED and Lewan MD. In (eds): Organic acids in geological processes: New York Springer-Verlag, p.319-354.

Giordano, T.H. and Kharaka, Y.K. (1994) Organic ligand distribution and speciation in sedimentary basin brines diagenetic fluids and

related ore solutions in Parnell J (ed) 1994 Geofluids: Origin Migration and Evolution of Fluids in Sedimentary Basins 175 Geological Society Special Publication No 78, p.175-202.

Giordano, T.H. (2000) Organic matter as a transport agent in ore-forming systems. In (ed): Giordano TH Kettler RM Wood SA Ore Genesis and Exploration: The Roles of Organic Matter Reviews in Econ. Geol., v.9, p.133-155.

Glikson, M., Golding, S.D., Boreham, C.J. and Saxby, J.D. (2000) Mineralisation in eastern Australia coals: a function of oil generation and primary migration In Glikson M and Mastalerz M (eds) OM and Mineralisation 2000 Kluwer Academic Publishers. p.314-326.

Haas, J. and Hámor G. (1998) Magyarország területe szerkezetfejlődésének összefoglalása, in. Borezi I. és Jámbor Á. (szerk.) (1998) Magyarország geológiai képződményeinek rétegtana, MOL Rt.-MÁFI kiadvány, Budapest, p.45-55. (Hungarian)

Haas, J., Budai T., Csontos L., Fodor L. and Konrád Gy. (2010) Pre-Cenozoic geological map of Hungary, 1:500 000. Geol Inst Hung, Budapest

Hámor, T. (1994) The occurrence and morphology of sedimentary pyrite. Acta Geologica Hungarica, v.37/2-2, p.153-181.

Harrison, C.H. (1991) Electron microprobe analysis of coal macerals. Org. Geochem., v.17(4), p.439-449.

Henrique-Pinto, R., Barnes S., Savard D.D. and Mehdi S. (2015) Quantification of metals and semimetals in carbon-rich rocks: a new sequential protocol including extraction from humic substances. Geostandards and Geoanalytical Research, p.1-22.

Hower, J.C., Calder, J.H., Eble, C.F., Scott, A.C., Robertson, J.D. and Blanchard, L.J. (2000) Metalliferous coals of Westphalian A Joggins Formation, Cumberland Basin, Nova Scotia, Canada: petrology, geochemistry and palynology. Int. J. Coal Geol., v.42, p.185-206. doi: 10.1016/S0166-5162(99)00039-7

Idiz, E.F., Carlisle, D. and Kaplan, I.R. (1986) Interaction between OM and trace elements in a uranium rich bog, Kern County, California, U.S.A. Appl. Geochem., v.1, p.573-590. doi: 10.1016/0883-2927(86)90065-X

Jacob, H. (1989) Classification structure genesis and practical importance of natural solid bitumen ("migrabitumen"). Int. J. Coal Geol., v.11. p.65-79. doi: 10.1016/0166-5162(89)90113-4

Junussov, M. (2018) Characteristics, distribution and morphogenesis of gold-bearing sulfide minerals in the gold black shale deposit of Bakyrchik. International Multidisciplinary Scientific Geo Conference Surveying Geology and Mining Ecology Management, SGEM, v.18(1.1), p.643-650.

Junussov, M., Mádai, F. and Olivér, B. (2018) Sequential extraction of carbonaceous siltstone rock for multielement analysis by ICP OES. Contemporary Trends in Geoscience, v.7(2), p.145-152. doi: 10.2478/ctg-2018-0010.

Junussov, M., Mádai F. and Kristály F. (2019) A two-step sequential extraction for analyzing hardly accessible precious metals in sulphide ore-bearing sedimentary rocks. Journal of geological resources and engineering, v.7(1), p.32-38. doi: 10.17265/2328-2193/2019.01.004

Junussov, M., Madai F., Kristály F., Tóth T., Fintor K., Muránszky G., Prekob Á., Hámor-Vidó M. (2021) Preliminary analysis on roles of metal-organic compounds in the formation of invisible gold. Acta Geochimica, 40, p.1050-1072. doi: 10.1007/s11631-021-00494-y

Junussov, M. (2022) Geological and genetic model of metal-organic compounds formation in Late Palaeozoic organic-rich sediments, using examples from Hungary and Kazakhstan. Miskolc University, Manuscript, Thesis, p.141.

Junussov, M., Mohammad, A. and Longinos, S. (2024) Geochemical analysis of organic matter associated with gold in ore deposits: A study of Kazakhstan and Hungary. Acta Geochimica, p.3-13. doi: 10.1007/s11631-024-00710-5

Kádas, M. (1983). Analysis on trace elements in coals of Mecsek. Geological research. (A mecseki feketekőszén nyomelemvizsgálatának legújabb eredményei. Földtani Kutatás, in Hungarian), 26, 81-82.

Lakatos, J., Brown, S.D. and Snape, C.E. (1997) "Unexpectedly High Uptake of Palladium by Bituminous Coals," in Proceedings of ICCS'97 (DGMK, Essen, 1997), v.1, p.247-250.

Machovič, V., Havelcová M., Sýkorová I., Borecká L., Lapčák L., Mizera J., Kříbek B. and Krist P. (2021). Raman mapping of coal halos induced by uranium mineral radiation. Spectrochimica Acta Part A: Molecular and Biomolecular Spectroscopy, v.246, 118996. doi: 10.1016/j.saa.2020.118996

Migdisov, A.A., Guo, X., Xu, H., Williams-Jones, A.E, Sun, C.J., Vasyukova, O., Sugiyama, I., Fuchs, S., Pearce, K. and Roback, R. (2017) Hydrocarbons as ore fluids. Geochem Persp Let 5, p.47-52 DOI: 107185/geochemlet1745

Mukherjee, S. and Borthakur P.C. (2003) Effect of leaching high sulphur subbituminous coal by potassium hydroxide and acid on removal of mineral matter and sulphur. Fuel, v.82, p.783-788. doi: 10.1016/S0016-2361(02)00360-5

Nayak, B., Chakravarty S. and Bhattacharyya K.K. (2008) Invisible gold in the high-sulphur Tertiary coals of Northeast India. Current science, v.95(9), p.1334-1337.

Parnel, J., Kucha, H. and Landais, P. (1993). Bitumens in ore deposits. Special publication no. 9 of the Society for Geology Applied to Mineral Deposits, no. 9. ISBN 978-3-642-85808-6.

Raffensperger, J.P. and Garven G. (1995) The formation of unconformity-type uranium ore deposits. 2. Coupled hydrochemical modeling. Am. J. Sci., v.295, p.639-696.

Raiswell, R. (1982) Pyrite texture, isotopic composition and the availability of iron. Am. J. Sci., v.282, p.1244-1263. doi: 10.2475/ajs.282.8.1244

Rojkovic, I., Francu, J. and Caslabsky, J. (1992) Association of organic matter with uranium mineralisation in the Permian sandstones of the Western Carpathians. Geologica Carpathica, 43, 1, Bratislava, p.27-34.

Ross, R.L., Stuart, W.B. and Valeriy, V.M. (2011) Carbonaceous Sedimentary Source-Rock Model for Carlin-Type and Orogenic Gold Deposits. Econ. Geol., v.106, p.331-358. doi: 10.2113/econgeo.106.3.331

Santbrd, R.F. (1994) A quantitative model of ground-water flow during tormation of tabular sandstone uranium deposits. Econ. Geol., v.89, p.341-360. doi: 10.2113/gsecongeo.89.2.341

Seredin, V.V. (2007) Distribution and Formation Conditions of

Noble Metal Mineralization in Coal-Bearing Basins. 2007. ISSN 1075-7015, Geology of Ore Deposits, v.49(1), p.1-30. doi: 10.1134/S1075701507010011

Seredin, V.V., Finkelman R.B. (2008) Metalliferous coals: A review of the main genetic and geochemical types. Int. J. Coal Geol., v.76, p.253-289. doi: 10.1016/j.coal.2008.07.016

Simoneit, B.R.T. (1994) Lipid/bitumen maturation by hydrothermal activity in sediments of Middle Valley Leg 139 In: Mottl M David E Fisher A Slack J (eds) Proceedings of the ocean drilling program scientific results vol 139 Ocean Drilling Program College Station. p.447-465. doi: 10.2973/odp.proc.sr.139.237.1994

Simoneit, B.R.T. (2000) Alteration and migration processes of OM in hydrothermal systems and implications for metallogenesis In: Glikson M Mastalerz M (eds) OM and mineralisation: thermal alteration hydrocarbon generation and role in metallogenesis Kluwer Academic Publishers Dordrecht: p.13-37. doi: 10.1007/978-94-015-9474-5_2

Simoneit, B.R.T. (2018) Hydrothermal Petroleum In Wilkes H (ed) Hydrocarbons Oils and Lipids: Diversity Origin Chemistry and Fate Handbook of Hydrocarbon and Lipid Microbiology Springer International Publishing AG part of Springer Nature https://doiorg/101007/978-3-319-54529-5_16-2

Szalay, S. (1954) Enrichment of uranium in some brown coals in Hungary. Acta Geol. Acad. Sei. Hung., 2, 299-311; CA, 48, p.12629.

Szalay, A. (1969) Accumulation of uranium and other trace metals in coal and organic shales and the role of humic acids in these geochemical enrichments. Ark. Mineral. Geol., v.5(3), p.23-36.

Szederkényi, T., Haas, J., Nagymarosy, A. and Hámor, G. (2012) Geology and History of Evolution of the Tisza Mega-Unit. p. 103-149 Book: Geology of Hungary. Editors Roland Oberhänsli, Maarten de Wit, Francois M. Roure. doi: 10.1007/978-3-642-21910-8_2

Sýkorová, I., Kribek, B., Havelcová, M., Machovič, V., Spaldónov, A, Lapcák, L., Knesl, I. and Blázek, J. (2016) Radiation- and self-ignition induced alterations of Permian uraniferous coal from the abandoned Nov´ator mine waste dump (Czech Republic). International Journal of Coal Geology. DOI: 10.1016/j.coal.2016.08.002

Varshal, G.M., Velyukhanova, T.K., Chkhetiya, D.N., et al. (2000) Sorbtion on Humic Acids as a Basis for the Mechanism of Primary Accumulation of Gold and Platinum Group Elements in Black Shales. Litol. Polezn. Iskop. 35 (6), 605-612 [Lithol. Miner. Resour., v.35(6), p.538-545. doi: 10.1023/A:1026645431074

Varga, E., Bella, M. and Benocs, S.K. (1972) Comparative survey of the trends of trace elements concentration in Hungarian coal fields. Puhl. Hung. Min. Res. Inst., No. 15, p.221-236.

Virágh, K. and Vincze J. (1967) A mecseki uránérclelőhely képződésének sajátosságai. (Specialty of uranium deposit formation in the Western Mecsek; in Hungarian). Földtani Közlöny, 97/1, p.39-59.

Vincze, K. (1987) A mecseki felsőperm uránércesedésének vizsgálata modellkísérletekkel. Földt. Közlöny, Bull, of the Hungarian Geöl. Soc., v.117, p.347-373.

Ward, C.R. and Gurba, L.W. (1998) Occurrence and distribution of organic sulphur in macerals of Australian coals using electron microprobe techniques. Org. Geochem., v.28(11), p.635-647. doi: 10.1016/S0146-6380(98)00038-2

Wood, S.A. (1996) The role of humic substances in the transport and fixation of metals of economic interest (Au Pt Pd U V). Ore Geol. Rev., v.11, p.1-33. doi: 10.1016/0169-1368(95)00013-5